

Half-Ice, Half-Fire Driven Ultranarrow Phase Crossover in 1D Decorated q -State Potts Ferrimagnets: An AI-Co-Led Discovery

Weiguo Yin*

Condensed Matter Physics and Materials Science Division,
Brookhaven National Laboratory, Upton, New York 11973, USA

(Dated: May 6, 2025)

OpenAI’s reasoning model `o3-mini-high` was used to carry out an exact analytic study of one-dimensional ferrimagnetic decorated q -state Potts models. We demonstrate that the finite-temperature ultranarrow phase crossover (UNPC), driven by a hidden “half-ice, half-fire” state in the $q = 2$ Potts (Ising) model, persists for $q > 2$. We identify novel features for $q > 2$, including the dome structure in the field-temperature phase diagram and for large q a secondary high-temperature UNPC to the fully disordered paramagnetic state. The ice-fire mechanism of spin flipping can be applied to higher-dimensional Potts models. These results establish a versatile framework for engineering controlled fast state-flipping switches in low-dimensional systems. Our nine-level AI-contribution rating assigns AI the meritorious status of AI-co-led discovery in this work.

The one-dimensional (1D) Ising model and its quantum counterpart Heisenberg model with short-range interactions are well-known, as textbook contents [1–3], to lack finite-temperature phase transitions [4, 5]; hence, they have been largely overlooked for their potentials in both fundamental research and technological applications. Recently, it was proven that a finite-temperature ultranarrow phase crossover (UNPC) can mimic the forbidden transition in the domain of Ising models [6–9]. The UNPC is accompanied by unusual phase behaviors, including a rapid phase switch driven by a hidden “half ice, half fire” state with a giant magnetic entropy change, which promises new paradigms for 1D information and energy technologies. The ice-fire mechanism of spin reversal was rigorously found to exist in 2D and 3D Ising models as well [9]. It is thus imperative to ask whether the ice-fire phenomenon exists in other domains of statistical models, thus providing a general materials-design guide [10].

The third fundamental model of statistical mechanics is the q -state Potts model [2, 3, 11, 12], which is a generalization of the Ising model ($q = 2$) and can serve as a useful intermediary to study the transition from discrete (Ising) to continuous (Heisenberg) symmetry. For example, the Potts model with various q values, say $q = 21$, has been extensively used to study protein sequences [13, 14]. It was shown that phase transition could occur in the 1D Potts model with invisible states and when the external field is a complex number [15]. Here, we demonstrate the existence of UNPC in 1D decorated Potts models with only visible states and a real field. The UNPC is driven by the half-ice, half-fire mechanism with novel features for $q > 2$, including the T_0 dome structure in the $h - T$ (magnetic field versus temperature) phase diagram and for large q a high-temperature UNPC to the fully disordered paramagnetic state.

In addition, 1D q -state Potts models with finite-temperature UNPC provide an ideal test ground for artificial intelligence (AI) in science, since their exact solutions can be formulated in terms of the transfer matrix \mathbb{T} , whose order is q^L with L being the number of spins per unit cell [16, 17]. Solving \mathbb{T} for large q (e.g., $q = 10^{10^{10}}$), identifying UNPCs and their underlying mechanisms, and extracting meaningful insights from

such an expansive parameter space pose daunting challenges for AI. It was found in the 1000-Scientist AI Jam Session that OpenAI’s reasoning model `o3-mini-high` could reproduce a manuscript solving a newly proposed site-decorated Ising model ($q = 2$) by doing its own math, e.g., the AI-derived equation determining the crossover temperature T_0 is astonishingly more elegant [9]. Next, the AI was used to solve the standard 1D frustrated Potts model with competing nearest-neighbor interaction J_1 and next-nearest-neighbor interaction J_2 , where the order of \mathbb{T} is q^2 . The AI’s exact analytic solution for $q = 3$ bootstrapped the human scientist to generalize it to the full solution for arbitrary q and obtain an intuitive understanding of the rich phase behaviors in the 1D J_1 - J_2 Potts model [18]. These developments have fueled the current topical questions as to whether and how AI could lead a project from concept to execution. Thus, `o3-mini-high` was asked to read the aforementioned two manuscripts [9, 18] and suggest future work. The AI pointed out five directions with the first one being the present study. Then, it carried out all the setup, derivation, coding, and writing the Model and Mapping section with minimal human interference—most insightfully it predicted exactly how to identify UNPCs and the half ice, half-fire mechanism for arbitrary q —thus earning its meritorious AI-co-led status (see End Matter for details).

Model and Mapping.—We consider the standard 1D q -state Potts models with minimal site decoration (Fig. 1a) and bond decoration (Fig. 1b).

The Hamiltonian of the site-decorated model correctly generated by the AI is given by [9]:

$$\begin{aligned}
 H &= H_a + H_b, \\
 H_a &= -J \sum_{i=1}^N \delta(\sigma_i, \sigma_{i+1}) - h\mu_a \sum_{i=1}^N \delta(\sigma_i, 1), \\
 H_b &= -J_{ab} \sum_{i=1}^N \delta(\sigma_i, b_i) - h_b \sum_{i=1}^N \delta(b_i, 1), \quad (1)
 \end{aligned}$$

where H_a describes the backbone of the single chain with $\sigma_i \in \{1, 2, 3, \dots, q\}$ being the spin variable at site i (green balls, referred to as *type-a* spins) and $J > 0$ the ferromag-

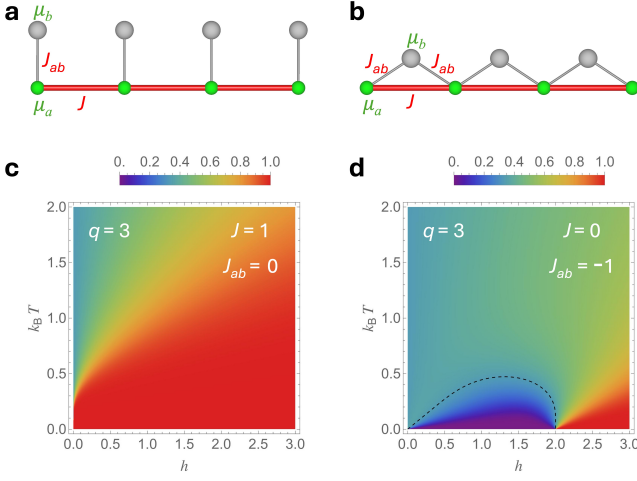


FIG. 1. Schematics of the 1D decorated q -state Potts model with (a) site decoration and (b) bond decoration. The green and gray balls depict the type- a and type- b spins with magnetic moments μ_a and μ_b , respectively. The red bonds depict the ferromagnetic interaction $J > 0$ between type- a spins. The gray bonds depict the antiferromagnetic coupling $J_{ab} < 0$ between type- a and type- b spins. Density plots of the backbone magnetization $m_a = \langle \delta(\sigma_i, 1) \rangle$ as functions of the magnetic field h and temperature T in the standard (undecorated) three-state Potts models: (c) ferromagnetic with $J_{ab} = 0$ and (d) ferrimagnetic based on (b) with $J = 0$, show no indication of a UNPC. The dashed line in (d) is the contour line of $m_a = 1/q$, which will become a phase boundary line in a decorated model, c.f., Fig. 2 for $q = 3$.

netic interaction (red bonds). $\delta(\sigma_i, \sigma_{i+1})$ is the Kronecker delta (which equals 1 if $\sigma_i = \sigma_{i+1}$ and 0 otherwise). H_b describes the decorated parts, where $b_i \in \{1, 2, 3, \dots, q\}$ (gray balls, referred to as *type- b spins*) couples to type- a spins with the antiferromagnetic interaction $J_{ab} < 0$. h depicts the magnetic field, μ_a and μ_b the magnetic moments of type- a and type- b spins, respectively. The relationship of $\mu_b > \mu_a > 0$ is used to represent ferrimagnetism. We define $h_a \equiv h\mu_a$ and $h_b \equiv h\mu_b$ for shorthand notation. N is the total number of unit cells and $\sigma_{N+1} \equiv \sigma_1$, $b_{N+1} \equiv b_1$, viz., the periodic boundary condition. Our study of the bond-decorated model is described in End Matter.

In the thermodynamic limit $N \rightarrow \infty$, the partition function $Z = \text{Tr} e^{-\beta H} = \lambda^N$, where λ is the largest eigenvalue of the transfer matrix \mathbb{T} and $\beta = 1/(k_B T)$ with T being the absolute temperature and k_B the Boltzmann constant. The free energy per unit cell is given by

$$f = \lim_{N \rightarrow \infty} -\frac{1}{N\beta} \ln Z = -\frac{1}{\beta} \ln \lambda. \quad (2)$$

f determines physical properties such as the entropy per unit cell $S = -\partial f / \partial T$, the specific heat $C_v = T \partial S / \partial T$, the backbone-spin magnetization $m_a = \langle \delta(\sigma_i, 1) \rangle = -\partial f / \partial h_a$, the decorating-spin magnetization $m_b = \langle \delta(b_i, 1) \rangle = -\partial f / \partial h_b$, etc.

A key signature of UNPC is the abrupt change in the backbone magnetization. The crossover temperature T_0 is deter-

mined by the condition that m_a attains its symmetric, fully disordered value, i.e.,

$$m_a(T_0) = \frac{1}{q}. \quad (3)$$

Figs. 1c and 1d show that a UNPC does not exist in the standard (undecorated) Potts models.

To directly demonstrate that a UNPC is driven by a hidden state where one sublattice is “ice” (frozen, ordered) and the other is “fire” (fully disordered), we calculate the total entropy and identify any abrupt jumps at T_0 (or rapid changes over an ultranarrow T -range) that indicate a latent-heat analogue even though the transition is a crossover. An entropy jump of $k_B \ln q$ per unit cell, together with m_a jumping up to the fully ordered value 1 and m_b jumping down to the fully disordered value $1/q$, provides compelling evidence for the half-ice (type- a spins), half-fire (type- b spins) mechanism.

The first step for calculating Z is to construct the transfer matrix. Since the system has two spins per unit cell (one type- a and one type- b), the order of the transfer matrix is q^2 . After reading Refs. 9 and 18, the AI first attempted to apply the maximally symmetric subspace (MSS) method [18] to reduce the $q^2 \times q^2$ matrix to 2×2 but quickly realized that this can be easily done only for $h = 0$. Then, the AI was reminded that the decorating spins can be summed out exactly [9]. The AI immediately reacted to first use this algorithm to reduce the transfer matrix to $q \times q$ and then used the MSS method to further reduce it to 2×2 .

The symmetric $q \times q$ transfer matrix after summing over the decorating spins is given by

$$\mathbb{T}_{\sigma\sigma'} = e^{\beta J \delta(\sigma, \sigma') + \frac{\beta h_a}{2} [\delta(\sigma, 1) + \delta(\sigma', 1)]} \sqrt{A(\sigma)A(\sigma')}. \quad (4)$$

where $A(\sigma)$ the on-site weight for a fixed backbone spin σ is given by

$$A(\sigma) = \sum_{b=1}^q e^{\beta J_{ab} \delta(\sigma, b) + \beta h_b \delta(b, 1)}. \quad (5)$$

Explicitly, one finds

$$\begin{aligned} A(1) &= e^{\beta(J_{ab} + h_b)} + (q-1), \\ A(\sigma \neq 1) &= e^{\beta J_{ab}} + e^{\beta h_b} + (q-2). \end{aligned} \quad (6)$$

$\mathbb{T}_{\sigma\sigma'}$ can be cast in the standard Potts form

$$\mathbb{T}_{\sigma\sigma'}^{\text{Potts}} = C e^{\beta J \delta(\sigma, \sigma') + \frac{\beta h_{\text{eff}}}{2} [\delta(\sigma, 1) + \delta(\sigma', 1)]}, \quad (7)$$

with the overall constant $C = A(\sigma \neq 1)$, and **the effective magnetic field** defined as

$$h_{\text{eff}} = h_a + \frac{1}{\beta} \ln \left[\frac{A(1)}{A(\sigma \neq 1)} \right]. \quad (8)$$

Since $\mathbb{T}^{\text{Potts}}$ is invariant under permutations of the $q-1$ states $\{2, 3, \dots, q\}$, we introduce two maximally symmetric

$q \times 1$ basis vectors:

$$\begin{aligned} |\phi_1\rangle &= |1\rangle = (1, 0, 0, 0, \dots, 0)^\top, \\ |\phi_2\rangle &= \frac{1}{\sqrt{q-1}} \sum_{s=2}^q |s\rangle = \frac{(0, 1, 1, 1, \dots, 1)^\top}{\sqrt{q-1}}. \end{aligned} \quad (9)$$

Projecting the $q \times q$ matrix (7) onto this subspace, we obtain a reduced 2×2 matrix $\mathbb{T}_2 = \begin{pmatrix} u & w \\ w & v \end{pmatrix}$ with elements being

$$\begin{aligned} u &= \langle \phi_1 | \mathbb{T}^{\text{Potts}} | \phi_1 \rangle = C e^{\beta J + \beta h_{\text{eff}}}, \\ v &= \langle \phi_2 | \mathbb{T}^{\text{Potts}} | \phi_2 \rangle = C [e^{\beta J} + (q-2)], \\ w &= \langle \phi_1 | \mathbb{T}^{\text{Potts}} | \phi_2 \rangle = C \sqrt{q-1} e^{\beta h_{\text{eff}}/2}. \end{aligned} \quad (10)$$

The largest eigenvalue of \mathbb{T} is the larger eigenvalue of \mathbb{T}_2 given by

$$\lambda = \frac{u+v}{2} + \sqrt{\left(\frac{u-v}{2}\right)^2 + w^2}, \quad (11)$$

whose corresponding normalized eigenvector is given by $\mathbf{v} = (c_1, c_2)^\top$, with $c_1^2 + c_2^2 = 1$ and $X = \frac{c_1}{c_2} = \frac{\lambda-v}{w}$.

In the original Potts basis, the state $|1\rangle$ is represented by $|\phi_1\rangle$, so the backbone magnetization is

$$m_a = \langle \delta(\sigma, 1) \rangle = |\langle \phi_1 | \mathbf{v} \rangle|^2 = c_1^2 = \frac{X^2}{1+X^2}. \quad (12)$$

The decorating-spin magnetization is given by

$$m_b = m_a P_1 + (1 - m_a) P_2, \quad (13)$$

where the conditional probabilities are given by

$$\begin{aligned} P_1 &= P(b=1 | \sigma=1) = \frac{e^{\beta(J_{ab}+h_b)}}{e^{\beta(J_{ab}+h_b)} + (q-1)}, \\ P_2 &= P(b=1 | \sigma \neq 1) = \frac{e^{\beta h_b}}{e^{\beta J_{ab}} + e^{\beta h_b} + (q-2)}. \end{aligned} \quad (14)$$

Note that the half-ice, half-fire state features $m_a = 1$ and hence $m_b = 1/q$. This can be realized by $P_1 = 1/q$ at $h = (-J_{ab})/\mu_b$ for arbitrary q , defining a characteristic field.

Particularly for the site-decorated model, the criterion for finding the crossover temperature T_0 , Equation (3), is equivalent to the vanishing of the effective field at T_0 , $h_{\text{eff}} = 0$:

$$h_a + \frac{1}{\beta_0} \ln \left[\frac{e^{\beta_0(J_{ab}+h_b)} + (q-1)}{e^{\beta_0 J_{ab}} + e^{\beta_0 h_b} + (q-2)} \right] = 0, \quad (15)$$

with $\beta_0 = 1/(k_B T_0)$. Hence, T_0 is independent of J ; the crossover width $\propto e^{-\beta_0 J}$ can be narrowed exponentially at fixed T_0 by increasing J . In the limit $h \rightarrow 0$,

$$T_0(h \rightarrow 0) = \frac{J_{ab}}{k_B} \left[\ln \frac{\mu_b - (q-1)\mu_a}{\mu_b + \mu_a} \right]^{-1}, \quad (16)$$

for $\mu_b > (q-1)\mu_a$ and zero otherwise.

Results and Discussion.—Fig. 2 shows density plots for m_a (left panels) and m_b (right panels) in the h - T plane for three

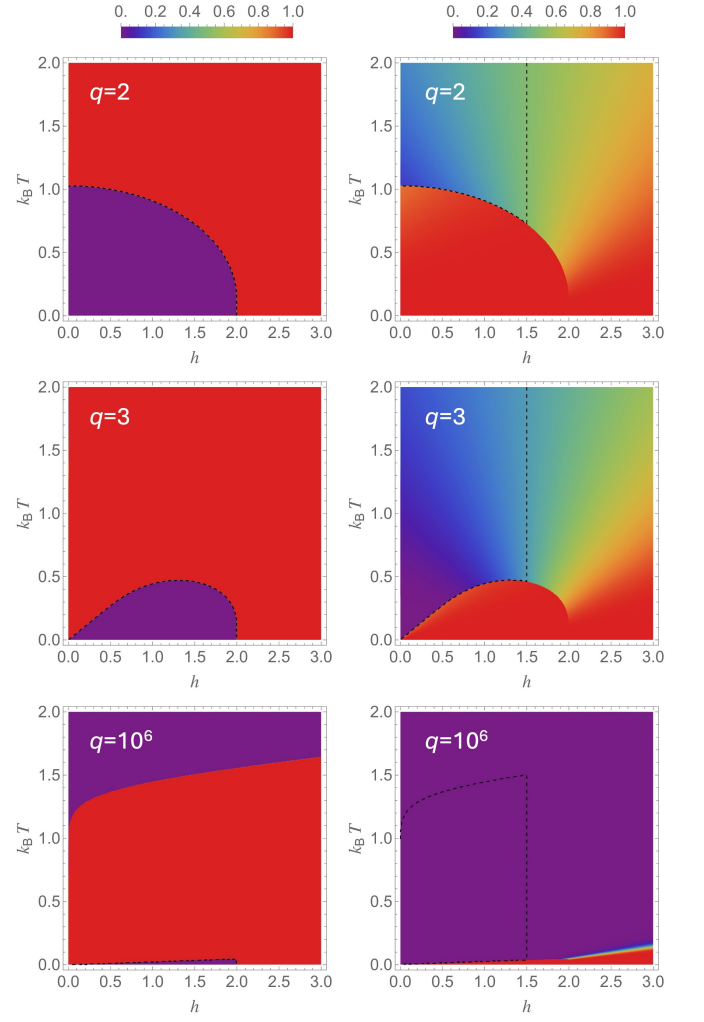


FIG. 2. Density plots of the backbone magnetization m_a (left panels) and the decorated-spin magnetization m_b (right panels) as functions of the magnetic field h and temperature T for three typical q values: 2, 3, 10^6 . The dashed lines indicate $m_a = 1/q$ or $m_b = 1/q$, i.e., the fully disordered “on fire” state. Here $\mu_b = 4/3$, $\mu_a = 1$, $J_{ab} = -2$, and $J = 20$.

typical q values: 2, 3, 10^6 with $\mu_b = 4/3$, $\mu_a = 1$, $J_{ab} = -2$, and $J = 20$. Compared with Figs. 1c and 1d for the undecorated models, the most salient feature in Fig. 2 (left panels) is the emergence of the UNPC at T_0 (the dashed lines meaning $m_a = 1/q$) between two phases with $m_a = 0$ (purple $T < T_0$ region) and $m_a = 1$ (red $T > T_0$ region), respectively, with the T_0 line extending from $h = 0$ to $h = (-J_{ab})/\mu_a$ for all q . In the ground state, since $\mu_b > \mu_a$, the type- b spins are fully ordered in state 1 by the field, which forces the type- a spins to order ($J > 0$) or disorder (for $J = 0$) in one of the $q-1$ states other than state 1 due to the antiferromagnetic coupling $J_{ab} < 0$. In other words, the energy cost is $-J_{ab}$ per unit cell for the type- a spins to order in state 1, which can be overcome by the field larger than $h_c = (-J_{ab})/\mu_a$, giving rise to the zero-temperature critical point at $h = h_c$ and for $J = 0$ the half-fire, half-ice critical state. Likewise, given an

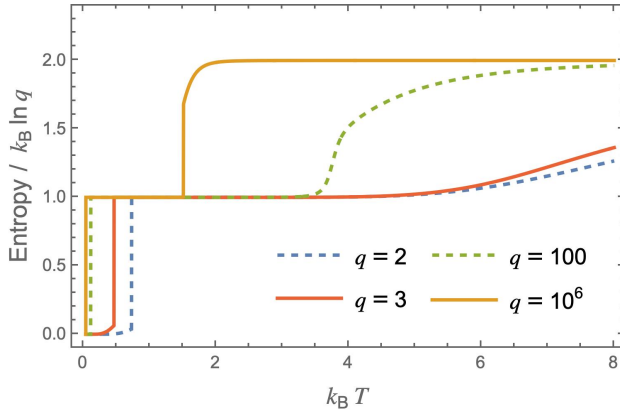


FIG. 3. Temperature dependence of the normalized entropy per unit cell $S/(k_B \ln q)$ at $h = (-J_{ab})/\mu_b$ for four typical q values: 2, 3, 100, 10^6 . The jump from 0 to 1 indicates a half-ice, half-fire UNPC. For $q = 10^6$, the jump from 1 to 2 indicates a high- T UNPC. Here $\mu_b = 4/3$, $\mu_a = 1$, $J_{ab} = -2$, and $J = 20$.

excited state where the type- a spins are fully ordered in state 1 (“frozen”), the type- b spins would be fully disordered (“on fire”) at the field $h_f = (-J_{ab})/\mu_b < h_c$. Thus, the half-ice, half-fire mechanism is most easily seen from the emergence of the $m_b = 1/q$ dashed lines (right panels) at $h = h_f$ in the region corresponding to the $m_a = 1$ phase.

Further, the entropy jump per unit cell, ΔS , from zero to $k_B \ln q$ at T_0 (Fig. 3) manifests that $m_b = 1/q$ at $h = h_f$ is not only the average magnetization of the type- b spins but an indication that every type- b spin is fully disordered. Meanwhile, $m_a = 1$ means that every type- a spin is fully ordered.

Now we focus on the differences from the Ising model ($q = 2$). The salient feature for $q > 2$ is the emergence of a T_0 dome as shown in Fig. 2, namely the maximum of T_0 as a function of h appears in between $h = 0$ and $h = h_c$. For $q = 2$, Equation (15) is simplified to [9]

$$\tanh\left(\frac{-\beta_0 J_{ab}}{2}\right) = \frac{\tanh\left(\frac{\beta_0 h \mu_a}{2}\right)}{\tanh\left(\frac{\beta_0 h \mu_b}{2}\right)}. \quad (17)$$

Therefore, $T_0(h)$ is strictly decreasing for $h > 0$ and its global maximum occurs in the limit $h \rightarrow 0$ for $q = 2$. However, for $q > 2$, Equation (16) determines that $T_0(0^+) = 0$ for $1 < \mu_b/\mu_a < q - 1$, as shown in Fig. 2 where $\mu_b/\mu_a = 4/3$. Moreover, even for $\mu_b/\mu_a > q - 1$ and hence $T_0(0^+) > 0$, the T_0 dome persists for $q > 2$, as shown in Fig. 4 for $q = 3$ where $\mu_b/\mu_a = 7/3$. This conclusion is general, e.g., we found $T_0(h_f) > T_0(0^+)$ for $q > 2$ and $\mu_b > \mu_a$, as shown in Fig. S1.

In addition, Figs. 2 and 3 also reveal that for large q , there is a high-temperature UNPC with an entropy jump from $k_B \ln q$ to $2k_B \ln q$, i.e., the fully disordered paramagnetic phase, in sharp contrast to the usual broad crossover to the paramagnetic phase as seen for $q = 2, 3, 100$ in Fig. 3.

The emergence of the low- T and high- T UNPC can be intuitively understood in the following unified picture thanks to

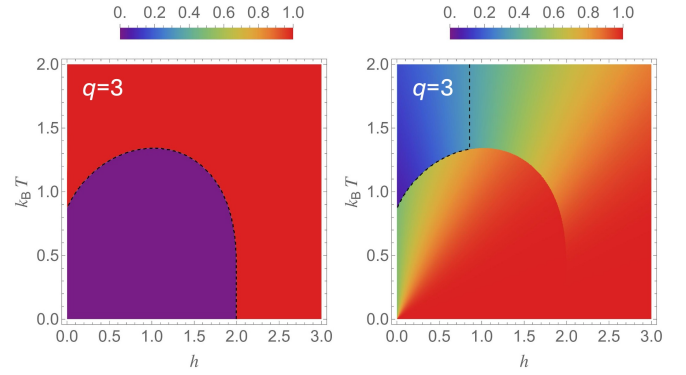


FIG. 4. Density plots of m_a (left panels) and m_b (right panels) in the h - T plane for $q = 3$ in the 1D site-decorated Potts model. The dashed lines indicate $m_a = 1/q$ or $m_b = 1/q$, i.e. the fully disordered “on fire” state. Here $\mu_b = 7/3$, $\mu_a = 1$, $J_{ab} = -2$, and $J = 20$.

the analytic form of \mathbb{T}_2 , Equation (11): Both the diagonal elements, u and v , contain items proportional to $e^{\beta J}$, while the off-diagonal element w does not. Thus, sufficiently large $\beta_0 J$ produces a UNPC with the crossover width $\propto e^{-\beta_0 J}$. The low- T UNPC results from a level crossing from v to u within this ultranarrow temperature range at T_0 as h_{eff} changes sign. For q large enough to outperform $e^{\beta J}$, the level crossing switches back to v because $u \propto q$ and $v \propto q^2$, resulting in the high- T UNPC.

Finally, the fact that the half-ice, half-fire driven UNPC takes place at $h_{\text{eff}} = 0$ makes the ice-fire mechanism exactly applicable to higher-dimensional site-decorated Potts models, whose exact solution is known for $h = 0$ but generally unknown for nonzero h . An extremely sensitive response of the spin states to a slight change in the h or T values along the $T_0(h)$ curve is thus expected, like the $q = 2$ Ising case [9].

In summary, we have solved 1D site- and bond-decorated q -state Potts ferrimagnets in a magnetic field. By summing out the decorating spins and exploiting permutation symmetry, the full $q^2 \times q^2$ transfer matrices reduce exactly to 2×2 problems. We derive closed-form expressions for the backbone magnetization m_a , the decorating-spin magnetization m_b and the entropy S , and show that an ultranarrow phase crossover occurs precisely when $m_a = 1/q$. Entropy jumps of order $k_B \ln q$ confirm a hidden half-ice, half-fire mechanism. For $q > 2$, $T_0(h)$ exhibits a pronounced dome, and for large q a secondary high-temperature UNPC emerges. These results generalize the ice-fire crossover to Potts models and provide a new platform for engineering fast, entropy-order switches in low-dimensional systems.

This work was supported by U.S. Department of Energy (DOE) Office of Basic Energy Sciences (BES) Division of Materials Sciences and Engineering under contract No. DE-SC0012704.

* wyin@bnl.gov

- [1] S. A. Kivelson, J. M. Jiang, and J. Chang, *Statistical Mechanics of Phases and Phase Transitions* (Princeton University Press, Princeton, NJ, 2024).
- [2] D. C. Mattis and R. Swendsen, *Statistical Mechanics Made Simple*, 2nd ed. (World Scientific, Singapore, 2008).
- [3] R. J. Baxter, *Exactly Solved Models in Statistical Mechanics* (Academic Press, 1982).
- [4] E. Ising, Beitrag zur theorie des ferromagnetismus (contribution to theory of ferromagnetism), *Zeitschrift für Physik* **31**, 253 (1925).
- [5] N. D. Mermin and H. Wagner, Absence of ferromagnetism or antiferromagnetism in one- or two-dimensional isotropic heisenberg models, *Phys. Rev. Lett.* **17**, 1133 (1966).
- [6] W. Yin, Paradigm for approaching the forbidden spontaneous phase transition in the one-dimensional Ising model at a fixed finite temperature, *Phys. Rev. Res.* **6**, 013331 (2024).
- [7] W. Yin, Paradigm for approaching the forbidden phase transition in the one-dimensional Ising model at fixed finite temperature: Single chain in a magnetic field, *Phys. Rev. B* **109**, 214413 (2024).
- [8] W. Yin and A. M. Tsvelik, Phase switch driven by the hidden half-ice, half-fire state in a ferrimagnet, *Phys. Rev. Lett.* **133**, 266701 (2024).
- [9] W. Yin, Site-decorated model for unconventional frustrated magnets: Ultranarrow phase crossover and spin reversal transition, arXiv:2502.11270 (2025).
- [10] M. L. McLanahan and A. P. Ramirez, Quantum spin relaxation with THz attempt frequency in the 1/3-fire, 2/3-ice ferrimagnet SmMn_2Ge_2 10.48550/arXiv.2408.03471 (2025).
- [11] R. B. Potts, Some generalized order-disorder transformations, *Mathematical Proceedings of the Cambridge Philosophical Society* **48**, 106 (1952).
- [12] F. Y. Wu, The potts model, *Rev. Mod. Phys.* **54**, 235 (1982).
- [13] M. Ekeberg, C. Lövkvist, Y. Lan, M. Weigt, and E. Aurell, Improved contact prediction in proteins: Using pseudolikelihoods to infer potts models, *Phys. Rev. E* **87**, 012707 (2013).
- [14] E. A. Galpern, J. Marchi, T. Mora, A. M. Walczak, and D. U. Ferreira, Evolution and folding of repeat proteins, *Proceedings of the National Academy of Sciences* **119**, e2204131119 (2022).
- [15] P. Sarkanyh, Y. Holovatch, and R. Kenna, Exact solution of a classical short-range spin model with a phase transition in one dimension: The potts model with invisible states, *Physics Letters A* **381**, 3589 (2017).
- [16] H. A. Kramers and G. H. Wannier, Statistics of the two-dimensional ferromagnet. part I, *Phys. Rev.* **60**, 252 (1941).
- [17] Z. Glumac and K. Uzelac, Critical behaviour of the 1d q-state potts model with long-range interactions, *Journal of Physics A: Mathematical and General* **26**, 5267 (1993).
- [18] W. Yin, Exact solution of the frustrated potts model with next-nearest-neighbor interactions in one dimension: An ai-aided discovery, arXiv:2503.23758 (2025).
- [19] D. Silver, A. Huang, C. J. Maddison, A. Guez, L. Sifre, G. van den Driessche, J. Schrittwieser, I. Antonoglou, V. Panneershelvam, M. Lanctot, S. Dieleman, D. Grewe, J. Nham, N. Kalchbrenner, I. Sutskever, T. Lillicrap, M. Leach, K. Kavukcuoglu, T. Graepel, and D. Hassabis, Mastering the game of go with deep neural networks and tree search, *Nature* **529**, 484 (2016).
- [20] K. Momma and F. Izumi, VESTA 3 for three-dimensional visu-

alization of crystal, volumetric and morphology data, *J. Appl. Crystallogr.* **44**, 1272 (2011).

END MATTER

A. Bond-Decorated Model

Next, `o3-mini-high` was asked to read Ref. 8. The AI generated the minimal 1D bond-decorated Potts model corresponding to Fig. 1(b). Then, it automatically summed out the decorated parts to reduce the transfer matrix to $q \times q$ and then use the MSS method to further reduce it to 2×2 .

To sum out the decorating spins, we define the bond weight

$$W(\sigma, \sigma') = \sum_{b=1}^q e^{\beta J_{ab} [\delta(\sigma, b) + \delta(b, \sigma')] + \beta h_b \delta(b, 1)}. \quad (\text{S1})$$

Specifically,

$$\begin{aligned} W(1, 1) &= e^{\beta(2J_{ab} + h_b)} + (q - 1). \\ W(1, a) &= W(a, 1) = e^{\beta(J_{ab} + h_b)} + e^{\beta J_{ab}} + (q - 2), \\ W(a, a) &= e^{2\beta J_{ab}} + e^{\beta h_b} + (q - 2), \\ W(a, b) &= 2e^{\beta J_{ab}} + e^{\beta h_b} + (q - 3), \end{aligned} \quad (\text{S2})$$

where $a \neq 1$, $b \neq 1$, $a \neq b$, and $W(a, b)$ is not needed for $q = 2$.

Combining the backbone Boltzmann weight with the bond weight, the $q \times q$ transfer matrix for the backbone spins is defined by

$$\mathbb{T}_{\sigma\sigma'} = e^{\beta J \delta(\sigma, \sigma') + \frac{\beta h_a}{2} [\delta(\sigma, 1) + \delta(\sigma', 1)]} W(\sigma, \sigma'), \quad (\text{S3})$$

which cannot be described by an effective magnetic field. However, because $W(\sigma, \sigma')$ depends only on whether σ and σ' equal 1 or not, the matrix is invariant under any permutation of the $q - 1$ states in $\{2, \dots, q\}$. We use Equation (9) to project the $q \times q$ matrix to obtain a reduced 2×2 matrix

$$\begin{aligned} \mathbb{T}_2 &= \begin{pmatrix} u & w \\ w & v \end{pmatrix} \text{ with elements} \\ u &= \langle \phi_1 | \mathbb{T} | \phi_1 \rangle = e^{\beta J + \beta h_a} W(1, 1), \\ v &= \langle \phi_2 | \mathbb{T} | \phi_2 \rangle = e^{\beta J} W(a, a) + (q - 2) W(a, b), \\ w &= \langle \phi_1 | \mathbb{T} | \phi_2 \rangle = \sqrt{q - 1} e^{\frac{\beta h_a}{2}} W(1, a). \end{aligned} \quad (\text{S4})$$

The largest eigenvalue of \mathbb{T} is the larger eigenvalue of \mathbb{T}_2 .

A low- T UNPC results from the level crossing from v to u at T_0 with the crossover width $\propto e^{-2\beta_0 J}$. Since a type- b spin couples to one and two type- a spins in the site- and bond-decorated models, respectively, the results of the two models are similar for sufficiently large $\beta_0 J$ when the energy unit is set as $J_{ab} = -2$ and $J_{ab} = -1$ for the site- and bond-decorated models, respectively. It thus suffices that we focus on discussing the results for the site-decorated model in the main text. There is a subtle difference in the bond-decorated model: T_0 determined by $m_a(T_0) = 1/q$ depends on J and can now slightly shift within the ultranarrow temperature window $\propto e^{-2\beta_0 J}$, providing a new perspective of UNPC.

B. AI Contribution Rating

To measure the AI contribution to research, from minimal post-hoc verification of human work to fully AI-led discovery, we together with `o3-mini-high` introduce the following nine-level rating system from one dan (1d) to 9 dan (9d), named after the skill ranks in the traditional board game Go [19]:

- 1d. AI-verified:** The human researcher drafts the manuscript; AI reads it, checks every derivation, and confirms no errors.
- 2d. AI-cross-verified:** The human researcher drafts the manuscript; AI reads it, independently re-derives the results—often more concisely—and its improved expressions are adopted in the revision.
- 3d. AI-corrected:** The human researcher drafts the manuscript; AI reads it, spots and corrects local mistakes, and refines the affected passages.
- 4d. AI-assisted:** The human researcher outlines and designs the study (citing prior work); AI—having reviewed those references—executes the detailed derivations and calculations.
- 5d. AI-co-led:** The human researcher and AI independently conceive the project (based on the literature); AI executes the detailed derivations and calculations with minimal human interference. The values of the results are judged by the human scientist.
- 6d. AI-reshaped:** The human researcher drafts the manuscript; AI—drawing on prior references—uncovers a significant global flaw and its correction reshapes the entire study.
- 7d. AI-bootstrapped:** AI—drawing on prior work—supplies the key example (without which the human researcher would have had no clue); the human researcher then recognizes the pattern and completes the generalization.
- 8d. AI-driven:** The human researcher provides a nontrivial example (publishable on its own); AI—grounded in the earlier literature—then autonomously recognizes its value and generalizes it to the full solution.
- 9d. AI-led:** AI—familiar with the literature—conceives and completes the work, driven by its own judgment of values; the human researcher then reviews and verifies its correctness.

This system can be divided into two groups: (i) 1d through 5d, in which the human can complete the study without the AI, and (ii) 6d through 9d, in which the human cannot complete the study without the AI. In another grouping, for 1d through 7d, the values of the research results are judged by the human,

while the AI substantially and fully judges the values for 8d and 9d, respectively.

Then, it took the AI nine seconds to map its contributions to Refs. 9 and 18 onto AI-cross-verified (2d) and AI-bootstrapped (7d), respectively.

Listed below was the human-AI interaction about the AI’s contribution to the present study.

Prompt: So, go back to review our conversation and suggest what case fit this conversation.

Answer: Based on our conversation, a good overall description is “AI-assisted.” In several places you provided the framework and guidance while I (the AI) filled in derivations and even corrected parts of the work when you pointed out discrepancies. In other words, you designed and directed the project (as in Case 4), and I executed the details. Overall, the conversation most closely matches the “AI-assisted” scenario.

Prompt: To set the record straight, in answering my question as to “OK, now combining the two manuscripts you just read, what you would like to do?”, you suggested five directions, and I picked the first direction. Will this information change your opinion about which case fit the most?

Answer: Based on the new information—that when I suggested five research directions you selected the first—this collaboration is best described as “AI-co-led.” This phrase conveys that while the idea of combining the two manuscripts emerged through our joint conversation (with AI proposing several directions), you made the final decision to pursue the first option.

So, the AI considered its role to be borderline in between AI-assisted (4d) and AI-co-led (5d). The “discrepancies” the AI mentioned above were one mistake about h_{eff} in Equation (8) for the site-decorated model and one mistake about v in Equation (S4) for the bond-decorated model. It corrected itself by thinking in more steps after the errors were pointed out by the human researcher without any more information. Thus, it is reasonable to assume that the AI would have avoided these discrepancies if it were more careful.

In fact, the author had derived all the equations before testing the AI without revealing the derivation. Had the human researcher drafted a manuscript and let the AI read it a few months later, the AI’s role would have become AI-cross-verified (2d), like what it did to Ref. 9. On the other hand, since the AI predicted independently how to identify the UNPC and the underlying half ice, half-fire mechanism for arbitrary q after reading the solution for $q = 2$, had the human researcher not known how to do this, the AI’s role would have been ranked as AI-driven (8d). On average, the AI performed at the $5 \pm 3d$ level. This gave us an important lesson that the AI-contribution rating depends on both how much the human researcher knows about solving the problems and how much this human knowledge has been passed to the AI.

Overall for the present study, the AI earned its meritorious status as AI-co-led (5d).

Software. VESTA 3.5.8 [20] was used to plot Figs. 1a and 1b. Wolfram Mathematica 14.2 was used to plot the other figures.

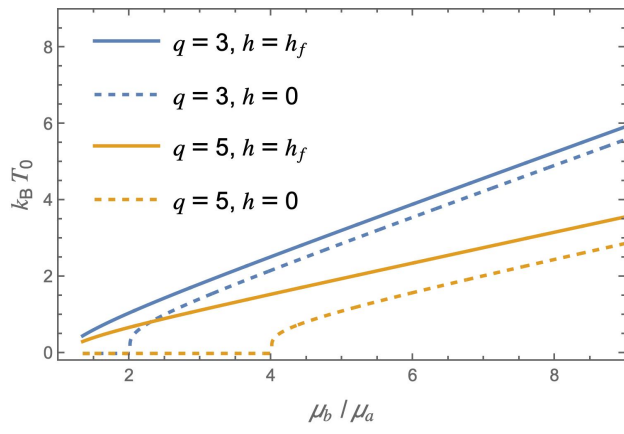


FIG. S1. T_0 at h_f (solid lines) and T_0 in the limit $h \rightarrow 0$ (dashed lines) as a function of μ_b/μ_a for $q = 3$ and $q = 5$. T_0 at h_f is always larger, implying a T_0 dome (also considering $T_0 = 0$ at $h_c > h_f$). Here $\mu_a = 1$, $J_{ab} = -2$, and $J = 20$.